



ELSEVIER

Available online at www.sciencedirect.com

SCIENCE @ DIRECT®

Nuclear Instruments and Methods in Physics Research A 522 (2004) 420–431

**NUCLEAR
INSTRUMENTS
& METHODS
IN PHYSICS
RESEARCH**
Section A

www.elsevier.com/locate/nima

Parallel plate chambers for monitoring the profiles of high-intensity pulsed antiproton beams

M. Hori*

CERN, EP Division, CH-1211 Geneva 23, Switzerland

Received 21 September 2003; accepted 3 November 2003

Abstract

Two types of beam profile monitor with thin parallel-plate electrodes have been used in experiments carried out at the Low Energy Antiproton Ring (LEAR) and Antiproton Decelerator (AD) of CERN. The detectors were used to measure non-destructively the spatial profiles, absolute intensities, and time structures of 100–300-ns-long beam pulses containing between 10^7 and 10^9 antiprotons. The first of these monitors was a parallel plate ionization chamber operated at gas pressure $P = 65$ mbar. The other was a secondary electron emission detector, and was operated in the ultra-high vacuum of the AD. Both designs may be useful in medical and commercial applications. The position-sensitive electrodes in these detectors were manufactured by a novel method in which a laser trimmer was used to cut strip patterns on metallized polyester foils.

© 2003 Elsevier B.V. All rights reserved.

PACS: 41.85.Qg; 07.77.Ka; 36.10.–k; 36.10.Gv

Keywords: Parallel plate ionization chamber; Secondary electron emission detector; Beam profile monitor; Antiprotonic helium atom

1. Introduction

In this paper, I report on two types of beam profile monitor, a parallel plate ionization chamber (PPIC) and a secondary electron emission detector. Both had parallel-plate electrodes made of metallized polyester foils. The PPIC was used in laser spectroscopy experiments on antiprotonic helium ($\bar{p}\text{He}^+$) atoms [1] carried out during the years 1995–1996 at the Low Energy Antiproton Ring (LEAR) of CERN. These atoms are composed of a helium nucleus, an antiproton, and an

electron, and have microsecond-scale lifetimes against annihilation. The experiments [2] involved stopping 200–300-ns-long beam pulses containing between 5×10^7 and 1×10^9 antiprotons in a cryogenic helium gas target, thereby producing between 1×10^6 and 3×10^7 metastable $\bar{p}\text{He}^+$ atoms. The PPIC was located upstream of the target, and was required to monitor non-destructively the spatial profile, absolute intensity, and time structure of each antiproton pulse arriving at the target. This meant that the PPIC had to be thin enough ($t_d = 45 \mu\text{m}$ of polyester in this case) to cause negligible energy loss and multiple scattering to the 21-MeV antiprotons traveling through the detector. The $\bar{p}\text{He}^+$ atoms were irradiated by a

*Tel.: +41-22-767-8306; fax: +41-22-767-3500.

E-mail address: masaki.hori@cern.ch (M. Hori).

laser beam tuned to one of their atomic transition frequencies, thereby causing the antiprotons to deexcite from stable, long-lived atomic orbits to unstable ones with short lifetimes against annihilation [1,2]. Knowledge of the spatial profiles of the antiproton beam detected by the PPIC was essential in ensuring an optimum overlap between the antiproton and laser beams.

These experiments ended in 1996 with the closure of LEAR [3,4], but were resumed in 1999 by the ASACUSA (Antiproton Spectroscopy And Collisions Using Slow Antiprotons) collaboration [5–13], now using the Antiproton Decelerator (AD) [14,15]. Here the PPIC was replaced with a new secondary electron emission detector, which required no gas for operation and could be placed directly in the ultra-high vacuum of the AD. The detector has been continuously operated with little maintenance during the years 1999–2003, and used in a high-precision laser spectroscopy experiment of $\bar{p}\text{He}^+$ which determined the antiproton's mass and charge to a fractional precision of 6×10^{-8} [7,8].

A considerable demand now exists for radiation detectors in commercial and medical applications, wherein targets such as semiconductors or cancer tumors are irradiated with high-intensity electron, proton or ion beams [16]. PPICs and secondary electron emission detectors such as those described here are ideal for measuring the spatial profiles and dosages of these beams; the detectors are relatively inexpensive and reliable, with low maintenance requirements and high resistance against radiation damage.

The purpose of this paper is to give a detailed description of the construction and readout electronics of these profile monitors, and show some typical results obtained at various intensities of the antiproton beam. The position-sensitive electrodes of these monitors were produced by a novel method in which a laser trimmer was used to cut strip patterns on metallized polyester foils. Signal lines were connected to each strip electrode by thick-film printing of metallic pastes. By using these efficient manufacturing techniques, a detector could be built within a few weeks at lower cost than those produced using conventional methods, and with improved reliability. These techniques

can also be used to produce foils with active areas $500 \text{ mm} \times 500 \text{ mm}$, and strip electrodes with a fine pitch of $p = 100 \text{ }\mu\text{m}$.

In Section 2, the construction of the PPIC and the methods to manufacture the position-sensitive electrodes are described. The electronic readout of the monitor is outlined in Section 3. The absolute intensities of the antiproton pulses were calibrated by a nuclear activation method described in Section 4. In Section 5, measurements carried out with the PPIC installed in the LEAR antiproton beam are reported. The secondary electron emission detector used at the AD, and some experimental results are described in Section 6.

2. Parallel plate ionization chamber (PPIC)

The PPIC consisted of three parallel polyester foils of $1.5\text{-}\mu\text{m}$ thickness—an anode foil, and two position-sensitive cathodes mounted at a distance of 2 mm on either side of it (Fig. 1). As indicated above, it was important to reduce the multiple scattering and range straggling introduced by the PPIC; the total thickness of material traversed by the antiprotons, including the vacuum windows, was equivalent to $t_d = 45 \text{ }\mu\text{m}$ of polyester foil. The construction was similar to those of parallel plate avalanche counters (PPACs) widely used in heavy ion accelerator facilities [17–20].

An ionization chamber [21] with parallel-plate electrodes was chosen rather than one with wires [22–24] for two reasons: (i) *linearity*: the former maintains a linear response even at high antiproton intensities where large numbers of electron–ion pairs are produced in the gas [25,26]. This is because the electrons and ions are not concentrated by strong, non-linear electric fields into small regions as is the case in wire chambers, where high charge densities occur near the wire surface [21,22], (ii) *timing response*: PPICs are characterized by fast timing response [17], since electrons created by primary ionization are immediately accelerated between the parallel-plate electrodes and induce a signal in them. This allows the time structures of the antiproton pulses to be measured with minimum distortion. In contrast, the electrons in wire chambers must first drift to

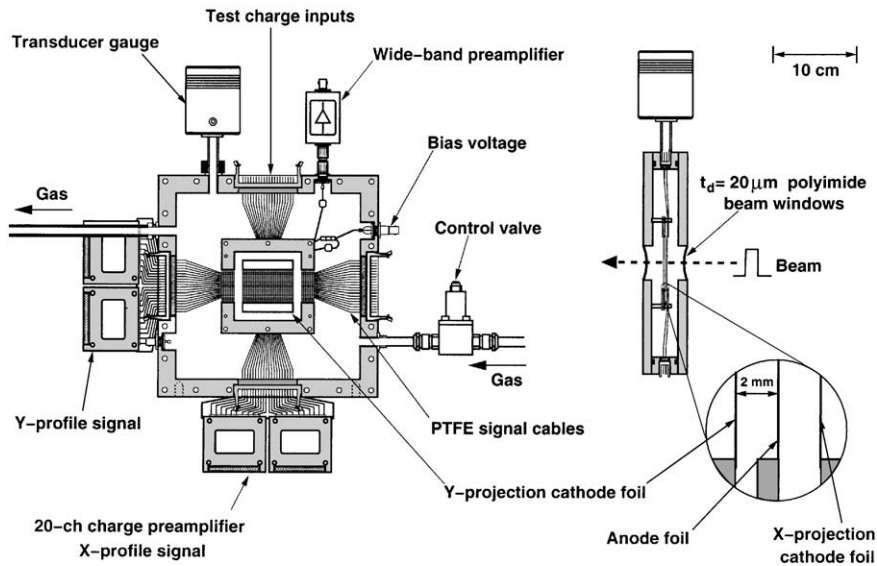


Fig. 1. Front and side cross-sectional views of the parallel plate ionization chamber. The detector consists of a pair of X- and Y-projection cathode foils and a common anode foil (see blow-up).

the proximity of the wires before producing a signal [22,24], which leads to a slower timing response.

The anode was manufactured by depositing 20-nm-thick layers of gold on the front and back sides of a 1.5- μm -thick polyester foil by sputtering in vacuum. The position-sensitive cathodes consisted of 20 segmented strips in each plane which provided the X- and Y-projections of the anti-proton beam [Figs. 2(a)–(c)], each strip being 0.92-mm wide with a 80- μm spacing between two neighboring strips. The patterns were produced by depositing a 20-nm-thick layer of gold uniformly across the entire surface of the polyester foil, and then selectively removing this gold layer using a laser trimmer.

A schematic drawing of the cutting process is shown in Fig. 2(d). A pulsed laser beam of wavelength $\lambda = 1064 \text{ nm}$ was emitted by a Q-switched, neodymium-doped yttrium-aluminum garnet (Nd:YAG) laser, and focused into a 80- μm -diam spot on the foil. By slowly scanning this spot along the surface of the foil using movable mirrors controlled by a computer, 80- μm -wide lines were drawn where the gold was vaporized and the underlying polyester exposed.

The polyester, being highly transparent, was undamaged by the laser. The laser energy had to be finely tuned according to the type of metal used and its thickness; at excessively high energies, small pinholes (typically $d = 10\text{--}30 \mu\text{m}$ in diameter) were burnt in the polyester, whereas at insufficient energies the gold layer could not be completely removed.

Two alternative methods of producing the patterned electrodes were also tested: (i) photolithography [27] and (ii) evaporation through a photomask. In the former method, a 100-nm-thick aluminum layer was sputtered onto a 1.5- μm -thick polyester foil. A pattern of 100- μm -wide strips with 400- μm spacings between each strip was printed on the aluminum using photoresist ink. After curing the photoresist, the foil was submerged in acid to selectively etch only the exposed areas of the aluminum surface. The foil was removed from the acid bath and the photoresist peeled off, thereby uncovering the strip electrodes. It was often found, however, that the strips so produced had uneven widths and jagged edges. In the evaporation method, a 200- μm -thick photomask with the desired pattern of strips cut into it was fixed on the surface of a polyester foil, and

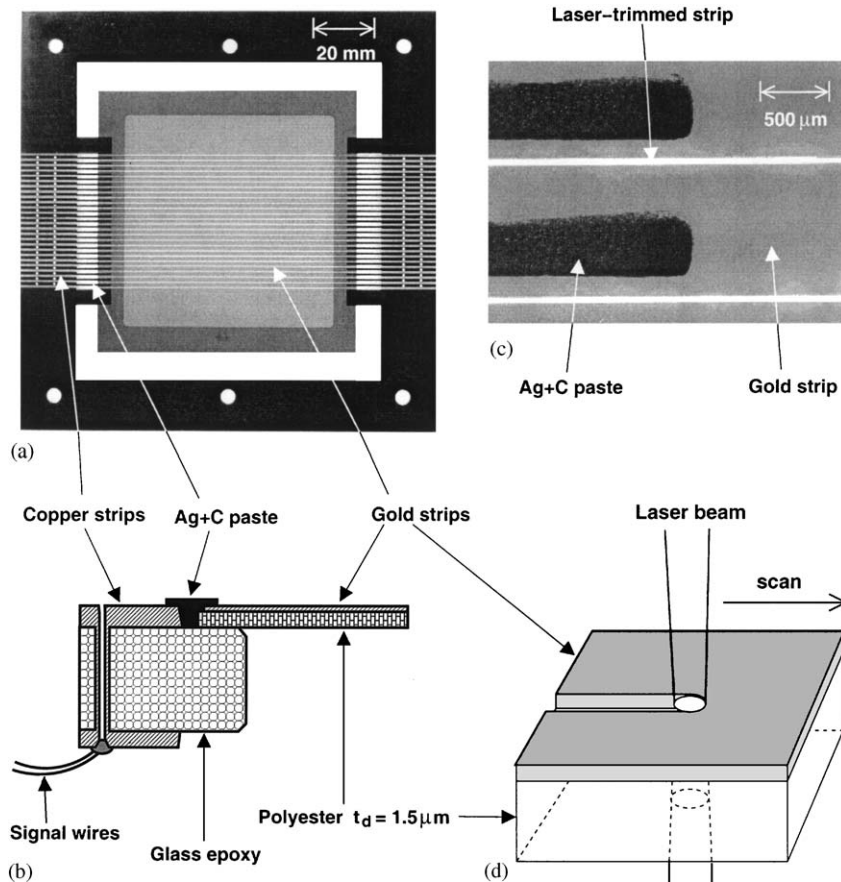


Fig. 2. Photograph of the position-sensitive cathode foil of the parallel plate ionization chamber (a). Cross-section of the foil, showing the connections between the gold strips on the 1.5- μm -thick polyester foil, and the copper strips on the glass-epoxy frame (b). Microscope photo of the connection (c). Schematic drawing showing the laser-trimming process used to produce the strip electrodes on the polyester foil (d).

gold was evaporated through the photomask. Although this method was successful, a photomask had to be made for each new electrode design. Laser trimming was ultimately found to be the easiest and most economical technique, since electrode foils with various patterns could be produced by simply reprogramming the trimmer.

The patterned foil was glued onto a glass-epoxy frame measuring $120\text{ mm} \times 120\text{ mm} \times 2\text{ mm}$ using an epoxy-based two-component cement (Cemedine 1565) with low viscosity. The frame had a $60\text{-mm} \times 60\text{-mm}$ opening in the center to allow the passage of antiprotons, and 20 copper strips were printed along its edges; these were

aligned to the positions of the gold strips on the polyester foil. Each copper strip was electrically connected to the corresponding gold one by printing a $200\text{-}\mu\text{m}$ -thick strip of epoxy-based silver-carbon paste (produced by Tanaka Kikin-zoku) to bridge the boundary between the two as shown in Fig. 2(b) and (c). The paste was cured by heating the electrodes to a temperature $T = 120^\circ\text{C}$.

The measurements of the antiproton beam were mainly carried out using the position-sensitive electrodes with a spatial resolution of 1 mm described above, but we also produced and tested electrodes with a pitch $p = 250\text{ }\mu\text{m}$ and active area

of 10 mm × 10 mm. The resolution of the laser trimmer ($\sim 50 \mu\text{m}$) and thick film printing ($\sim 25 \mu\text{m}$) techniques used here allowed strip electrodes with a minimum pitch $p = 100 \mu\text{m}$ to be manufactured.

The chamber was made of stainless steel and measured 200 mm × 200 mm × 30 mm (Fig. 1). Antiprotons entered through a 40-mm-diameter, 20- μm -thick polyimide window (Ube Industries Upilex-S), and exited through an identical window glued on the opposite side. The chamber was filled with a mixture of 90% argon and 10% methane (P10 gas) [24,28,29], at a low gas pressure $P = 65 \text{ mbar}$ which helped to minimize space-charge effects (see Section 5). New gas was constantly introduced into the chamber at a flow rate of 0.1 sccm using a regulated needle valve (MKS Instruments 248A valve and 250C controller), and pumped out by a dry membrane pump connected to the opposite side of the chamber. The gas pressure was measured to a precision of $\pm 0.2 \text{ mbar}$ using an absolute capacitance manometer (MKS Instruments Baratron 627), which had a heater to maintain the gas temperature at $T = 45^\circ\text{C}$. This reading was used to regulate the needle valve, thereby stabilizing the gas pressure with a precision of $\pm 0.5 \text{ mbar}$.

3. Electronic readout

During operation, the anode foil was biased at a voltage of $\sim 70 \text{ V}$ (Fig. 3), and the intensity and time structure of the antiproton pulses were derived by detecting the waveform of the signal induced on the anode. In order to sustain the large signals (electric charge $Q = 0.2\text{--}5 \text{ nC}$, see Section 5) induced by the antiproton pulses, a 100-nF storage capacitor was installed in parallel to the anode electrode. The anode signal was amplified by a wide-bandwidth amplifier with a frequency response $f = 5 \text{ kHz--}500 \text{ MHz}$, an input decoupling capacitor $C = 2.2 \mu\text{F}$, an input impedance $R = 25 \Omega$, and unit gain. The analog waveform was recorded using a digital oscilloscope (Hewlett Packard HP54542A) with an analog bandwidth $f = 500 \text{ MHz}$ and a digital sampling rate $f = 2 \text{ GHz}$.

The spatial profile of the beam was obtained by measuring the electric charge induced on the 40 strip electrodes on the two cathode foils. The strips were individually read out by charge-sensitive preamplifiers (Clear Pulse CS507) connected to them through 6.8-nF decoupling capacitors. Each preamplifier was packaged in a 40-mm-long hybrid integrated circuit, so that the required 40 preamplifier channels could be attached on the sides of the chamber. To obtain linear signals even at high antiproton intensities, the full-range capacities of the preamplifiers were adjusted to a high value $Q = 4\text{--}5 \text{ nC}$. This was done by installing 470-pF feedback capacitors between the input and output terminals of the preamplifiers (Fig. 3), thus reducing their charge-to-voltage conversion factors to $dV/dQ \sim 2 \text{ mV/pC}$.

Active filter amplifiers (Clear Pulse 4018A) with integrator and differentiator circuits, and a gain $g = 0.7$ were used to shape the signals into unipolar Gaussian pulses with a time constant $\tau = 2 \mu\text{s}$. These low-impedance signals were then transmitted over a distance $l = 20 \text{ m}$ to an electronics room located outside the experimental area. The signal amplitudes were here measured using peak-sensitive analog-to-digital converters (ADC, Hoshin C008) with 12-bit resolution. Voltage amplifiers with variable gain (Clear Pulse 4031) were used to adjust the signal levels so as to match the full range of the ADCs. Before the experiment, the ADC readings were absolutely calibrated by injecting into each position-sensitive electrode of the PPIC a 100-pC charge, which simulated the signal induced in the detector by the antiproton beam. This was done in the following way: a precision pulse generator (Ortec 448) equipped with a mercury-wetted relay produced a 1-ms-long voltage pulse with an amplitude of 1 V, and a rise time $\tau_r = 300 \text{ ns}$ which corresponded to the pulse-length of the antiproton beam. The generator output was converted into a charge signal using a 100-pF decoupling capacitor, and transmitted to each strip electrode through vacuum feedthroughs and signal cables located on the sides of the detector opposite the charge-sensitive preamplifiers (Fig. 1).

The ADC readings were transferred using a CAMAC-to-SCSI interface (Kinetics 3929) to a

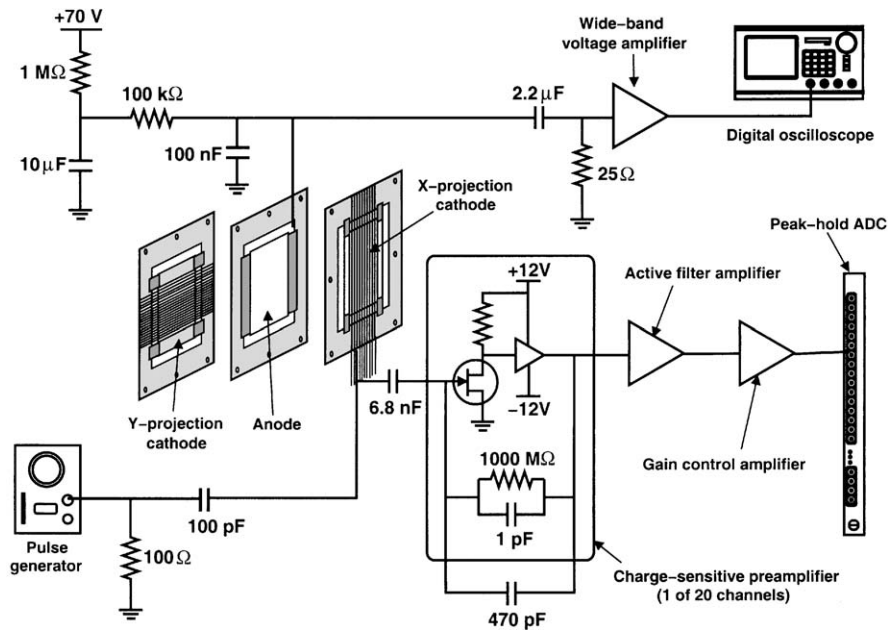


Fig. 3. Layout of the readout electronics of the parallel plate ionization chamber.

Digital Equipment VAXstation 4000 workstation, the latter running the VAX-VMS version 5.5 operating system and connected to the DECNET computer network of CERN. After the arrival of each antiproton pulse at the PPIC, its horizontal and vertical profiles were automatically displayed on the computer screen using the CERNLIB [30] and PAW [31] software packages. The same readout was also transmitted via network to the control room of LEAR, and used by its operators to adjust the trajectory of the antiproton beam.

4. Beam intensities measured by nuclear activation

These experiments required LEAR to be operated in 15-min-long cycles, which were initiated when $\sim 5 \times 10^9$ antiprotons at energy $K = 180$ MeV were injected into LEAR. The beam was debunched using radiofrequency cavities so that the antiprotons were distributed uniformly around the 78-m circumference of the ring. The antiprotons were then decelerated to an energy $K = 21$ MeV and cooled so that their momentum

spread was $\Delta p = 0.1\%$ and their transverse emittance $\Phi = (2 - 3)\pi$ mm mrad. A kicker magnet in the ring was activated for $\Delta t = 300$ ns [3], thereby diverting some 1×10^9 antiprotons towards the experiment [4]. Each successive activation of the magnet extracted a quarter of the beam circulating in the ring, the number of antiprotons $N_{\bar{p}}$ arriving at the experiment decreasing exponentially from 1×10^9 to 5×10^7 per pulse over ~ 10 extractions. After LEAR was thus emptied, a new cycle was started by replenishing the ring with a new stack of antiprotons. The number of antiprotons in LEAR was measured non-destructively using a DC beam current transformer and longitudinal Schottky pickup detector [32]. The intensity $N_{\bar{p}}$ of each antiproton pulse was deduced by measuring the decrease of these readings during the operation of the kicker magnet.

Ionization chambers provide an absolute measurement of the beam intensity if two conditions on the applied electric field E are met, (i) it is low enough so that little or no electron multiplication [29] occurs in the gas, i.e. the detector gain is close to unity, (ii) it is high enough so that space-charge

effects (see Section 5) are negligible. In order to evaluate these effects at various values of E , the beam intensity readings afforded by the PPIC was calibrated against absolute values $N_{\bar{p}}$ obtained by nuclear activation of an aluminum target.

When antiprotons are stopped in aluminum, they replace the atomic electrons and form antiprotonic aluminum ($\bar{p}\text{Al}$) atoms; these are destroyed within picoseconds as the antiprotons are absorbed by the nuclei. Experimental data [33] show that $F = (2.1 \pm 0.3)\%$ of these result in the production of the radioactive nuclei ^{24}Na , which has a half-life $T_{1/2} = 15$ h. Background due to ^{24}Na produced by processes other than antiproton annihilation is negligible small.

A 2-mm thick aluminum plate of 99.99% purity was placed immediately downstream of the PPIC, and an antiproton pulse stopped in it. The absolute yield of the characteristic gamma rays of ^{24}Na at energies $K = 1.37$ and 2.75 MeV emitted from the plate was measured using a germanium radiation monitor. Typical activation levels were $A = 10\text{--}200$ Bq, from which the number of antiprotons $N_{\bar{p}}$ stopped in the plate was deduced using the formula,

$$N_{\bar{p}} = \frac{A T_{1/2}}{F \log 2} \exp\left(\frac{\log 2}{T_{1/2}} t\right), \quad (1)$$

where t is the time elapsed between the irradiation of the aluminum and the measurement of its activation levels. The estimated values agreed to within 30% of the beam intensities derived using the DC beam transformer.

5. Measurements of antiproton beams using the PPIC

In Figs. 4(a)–(c), the anode signals induced by beam pulses containing $(0.5\text{--}1) \times 10^9$ antiprotons are shown, measured at a gas pressure $P = 65$ mbar and electric fields $E = 0.75, 7.5,$ and 75 V/mm (corresponding to bias voltages of 1.5, 15, and 150 V on the anode electrode, respectively). The signals are rectangular and 300 ns long, which agrees with the expected time structure of the antiproton beam. Following this main pulse, a weaker signal induced by the positive

ions drifting away from the anode was observed. This slow component lasted for ~ 100 μs until all the ions (which have typical drift velocities 1000 times lower than that of electrons) were collected.

The anode signal [Fig. 4(a)] observed at an electric field $E = 0.75$ V/mm was deformed, with slow rise and fall times ($\tau \sim 200$ ns). This reflected the low drift velocities $v \sim 10^4$ m/s [28,29] of the electrons traversing the 2-mm-interval between the cathode and anode foils. At a higher field $E = 7.5$ V/mm [Fig. 4(b)], the signal had faster rise and fall times ($\tau \sim 20$ ns) and provided a more accurate measurement of the rectangular time structure of the beam. At $E = 75$ V/mm [Fig. 4(c)], the fall time of the signal was similar to the value measured at $E = 7.5$ V/mm, whereas the rise time now increased to $\tau \sim 100$ ns. The reason for this increased rise time is not understood, but it may be due to a small amount of electron multiplication occurring in the gas [29].

The antiproton intensity $N_{\bar{p}}$ was non-destructively deduced from the charge collected by the anode, including both the fast and slow components induced by the electrons and ions, respectively. From experimental data on the energy-loss of antiprotons [34–37] and the work functions of argon and methane gas [22], it was estimated that a 21-MeV antiproton traversing the 4-mm-thick volume of P10 gas in the detector at a pressure $P = 65$ mbar produces ~ 30 ion pairs. A pulse containing $N_{\bar{p}} = 5 \times 10^7\text{--}1 \times 10^9$ antiprotons would thus produce ion pairs equivalent to a total charge $Q = 0.2\text{--}5$ nC and a spatial density $\rho = 5 \times 10^{10}\text{--}1 \times 10^{12}$ cm^{-3} , given the beam diameter $d = 3$ mm.

In Fig. 4(d), $N_{\bar{p}}$ estimated from the anode signal (plotted along the Y -axis) are compared with values estimated using nuclear activation (X -axis) described in Section 4. When the detector was operated at a low electric field $E = 0.75$ V/mm, the anode signal saturated at beam intensities $N_{\bar{p}} > 3 \times 10^8$. This is believed to be due to a space-charge effect which reduces the electric field in the gas, thereby decreasing the drift velocity of the ion pairs and causing them to be absorbed by the gas through recombination [22,25,26]. At the higher drift velocities corresponding to $E \geq 7.5$ V/mm, recombination is less likely, resulting in a linear

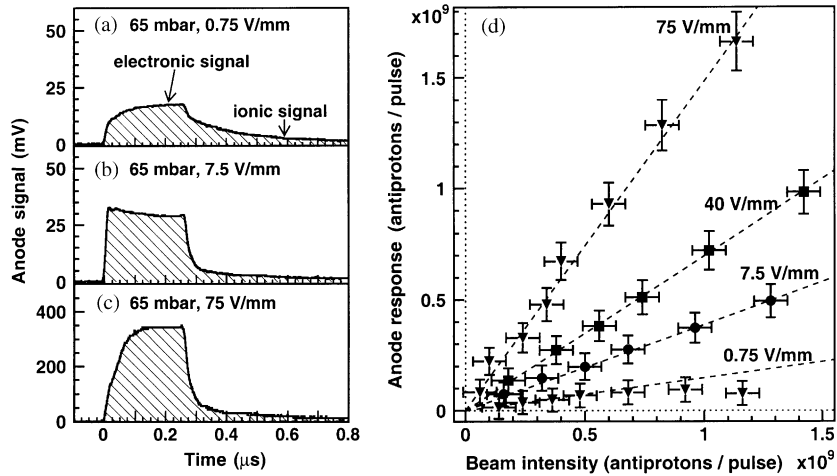


Fig. 4. Anode signals showing the time structure of antiproton pulses, measured at a gas pressure $P = 65$ mbar and electric fields $E = 0.75$ V/mm (a), 7.5 V/mm (b), and 75 V/mm (c). The number of antiprotons contained in individual pulses estimated using the charge collected at the anode (plotted along the Y -axis), as a function of the beam intensity derived from nuclear activation measurements (X -axis) (d).

response up to $N_{\bar{p}} = 1 \times 10^9$. At an electric field $E = 75$ V/mm, the charge collected by the anode was roughly equal to the value estimated as above for an ideal ionization chamber without gas recombination effects.

In Figs. 5(a) and (b), typical horizontal and vertical beam profiles of a single pulse containing 1×10^8 antiprotons are shown, looking downstream along the beam line. The beam centroid was determined by fitting Gaussian functions to the profiles. In Fig. 5(c), the horizontal and vertical centroids of 30 consecutive antiproton pulses measured during four LEAR cycles are shown. Each cycle consisted of 7–9 antiproton pulses, the intensities [Fig. 5(d)] of which decreased exponentially. The beam position systematically drifted by about 2 mm, moving from the upper-left quadrant of the detector (at the beginning of each cycle) to the lower-right quadrant (at the end of the cycle). This drift was presumably caused by small shifts in the orbits of the antiprotons in LEAR.

6. Secondary electron emission detector

The LEAR facility was closed at the end of 1996, and was replaced in 1999 by the AD. This

new machine produced 100-ns-long pulses containing $\sim 3 \times 10^7$ antiprotons at an energy $K = 5.3$ MeV and repetition rate $f = 0.01$ Hz. Laser spectroscopic studies of $\bar{p}\text{He}^+$ [7,9] were here continued by the ASACUSA collaboration, one of three experiments using the AD.

The PPIC described above had three disadvantages, namely (i) a substantial amount of hardware (high-pressure gas bottle, piping, pressure gauge, control valve, vacuum pump) were needed to constantly supply the detector with gas and regulate its pressure, (ii) the detector had two 20- μm -thick polyimide vacuum windows to separate the gas inside the chamber from the outside air. The windows would cause multiple scattering to the 5.3-MeV antiproton beam of AD, the effects of which would be larger compared to the higher-energy ($K = 21$ MeV) beams of LEAR, (iii) the amplitude of the PPIC signals had a strong dependence on the bias voltage and gas pressure, and saturation effects were observed at high intensities of the antiproton beam [Fig. 4(d)].

In the new series of experiments, these problems were solved by using a secondary electron emission detector instead of the PPIC [Figs. 6(a) and (b)]. Since it contained no gas, and consequently required no windows, this could be placed in the ultra-high vacuum chamber of the AD. The total

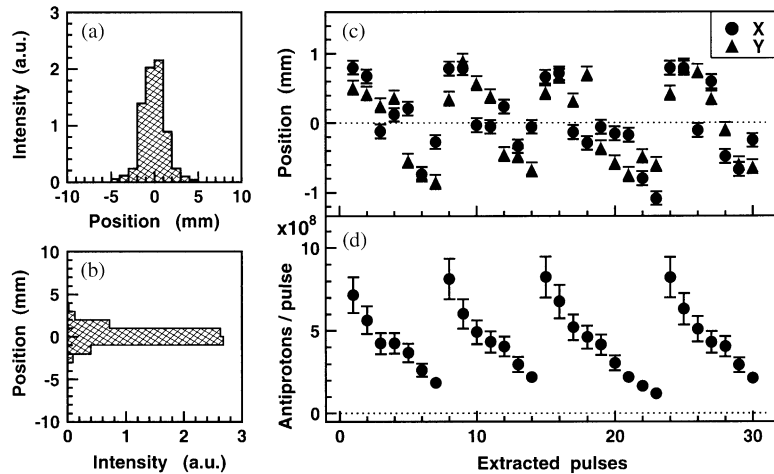


Fig. 5. Horizontal (a) and vertical (b) profiles of an antiproton beam pulse produced by LEAR, measured using the PPIC. The mean centroids (c) and intensities (d) of 30 consecutive antiproton pulses.

thickness of the detector was reduced to $t_d = 5 \mu\text{m}$ of polyester. Furthermore, the amplitudes of the signals produced by secondary electron emission were relatively unaffected by the bias voltage, and there were no saturation effects caused by gas recombination.

As before, the detector consisted of an anode foil and two position-sensitive cathode foils mounted on either side to provide the X- and Y-projections of the beam, with 4-mm spacings between each foil. The construction of the cathode foils [Fig. 6(b)] was similar to the ones of the PPIC described in Section 2, except in the following respects; (i) the electrodes were made of 50-nm thick layers of aluminum, which have a high yield of secondary electrons (see below), (ii) the supporting frame was made of ceramic, which had a low rate of outgassing and was compatible with the ultra-high vacuum of the AD.

The detector was placed in the last piece of vacuum pipe of the AD beam line, just in front of the cryogenic helium target [Fig. 6(a)]. To isolate the detector against electromagnetic interference which could be transmitted along the stainless-steel beam line, a ceramic break was inserted in the vacuum pipe between the detector and the AD. After baking the detector to a temperature $T = 100^\circ\text{C}$, the residual pressure in the chamber reached $P \sim 1 \times 10^{-9}$ mbar, mainly limited by the

outgassing from the polyester foils. The differential pumping provided by ion and turbo-molecular pumps installed further upstream along the beam line helped to maintain the pressure inside the AD at $P \sim 10^{-10}$ mbar.

When antiprotons struck the strip electrodes on the X- and Y-projection cathode foils, secondary electrons were emitted from their surfaces, and accelerated toward the anode foil which was biased at a voltage of 50–100 V. The spatial beam profile was obtained by measuring the electric charge ejected from each electrode using a charge-sensitive preamplifier (Fig. 3). The number of secondary electrons emitted per incident antiproton (i.e. the secondary electron emission yield γ_e) has never been measured, but it was assumed to be nearly equivalent to the corresponding values for protons with a kinetic energy $K = 5.3$ MeV. This assumption is based on the experimental observation that the energy loss dE/dX (which is known to be roughly proportional to γ_e) for antiprotons and protons at these energies are nearly equal [35,37]. The γ_e -values for 5-MeV protons striking pure gold, copper, and aluminum surfaces are about 0.5, 0.3, and 0.2, respectively [38]. Aluminum electrodes oxidized in air were used in the present detector, which have typical electron yields 3–5 times larger than in the pure aluminum case. Assuming a γ_e -value of 0.5–1 per antiproton, a

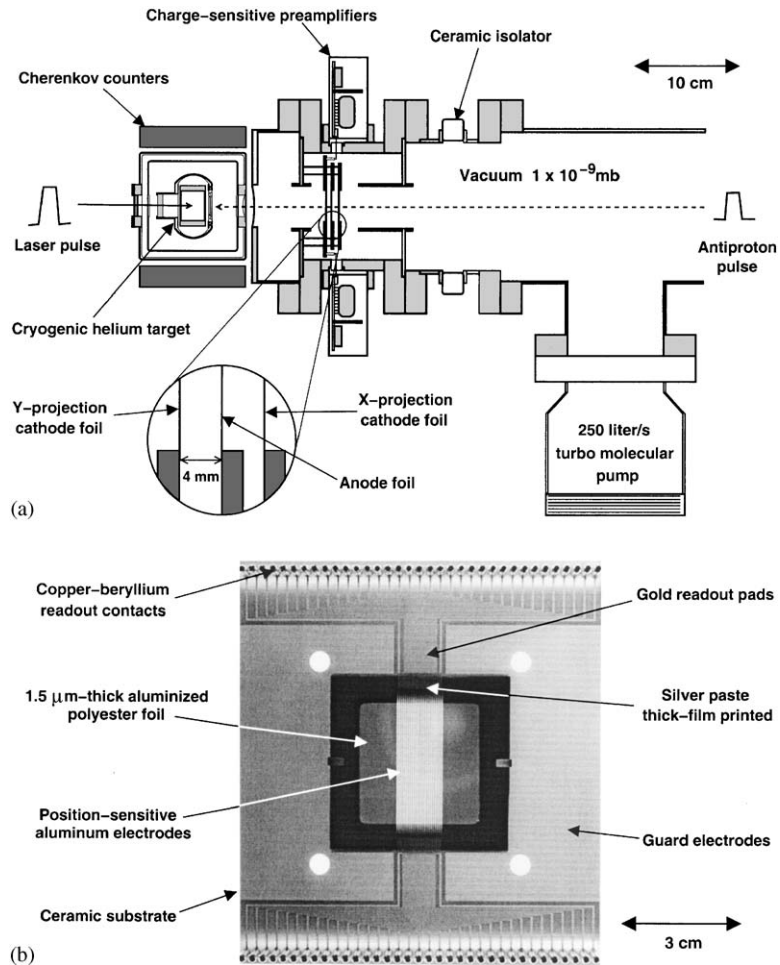


Fig. 6. Schematic drawing of the secondary electron emission detector used at the Antiproton Decelerator (AD) facility (a). Photograph of the position-sensitive cathode foil, which was compatible with the ultra-high vacuum of the AD (b).

single AD pulse containing 3×10^7 antiprotons would then induce a total charge $Q = 2\text{--}5$ pC. These signals are 1000 times weaker than those obtainable with the PPIC. In order to detect them, it was necessary to adjust the feedback capacitors of the preamplifiers to a value $C = 1$ pF, corresponding to charge-to-voltage conversion factors $dV/dQ \sim 1$ V/pC.

In Figs. 7(a) and (b), typical horizontal and vertical profiles of the AD beam measured using the secondary electron emission detector are shown, looking downstream along the beam line. The profiles were characterized by a dense core of

cooled antiprotons with a diameter $d = 5$ mm, surrounded by a large ($d > 20$ mm) halo containing antiprotons that were poorly cooled by the electron beam cooler of the AD [15]. This result was compatible with the emittances of the antiproton beam measured by other detectors located inside the AD [39]. The horizontal and vertical centroids of 30 consecutive antiproton pulses are plotted in Fig. 7(c), and show the spatial position of the beam fluctuating by about ± 2 mm in both planes. As shown in Fig. 7(d), the number of antiprotons $N_{\bar{p}}$ fluctuated by $\sim 20\%$ from pulse to pulse. The measured signal amplitudes are

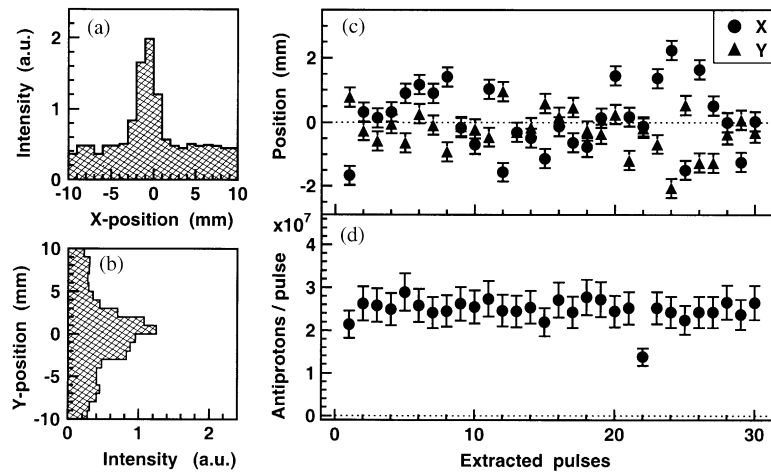


Fig. 7. Horizontal (a) and vertical (b) profiles of an antiproton beam pulse produced by the AD, measured using the secondary electron emission detector. Note large ($d > 20$ mm) beam halo containing antiprotons that were poorly cooled. The mean centroids (c) and intensities (d) of 30 consecutive antiproton pulses.

roughly compatible with the above assumptions on γ_e , and a signal-to-noise ratio of $S/N > 200$ was attained. Using these beams [which had a much higher stability than those of LEAR, Fig. 5(d)], the atomic transition frequencies of $\bar{p}\text{He}^+$ were measured to a fractional precision of 1.3×10^{-7} [7,8].

We have constructed an ionization chamber and secondary electron emission detector with thin parallel plate electrodes, and used them to measure the spatial profiles, absolute intensities, and time structures of high-intensity antiproton beam pulses with energies $K = 5.3\text{--}21$ MeV. In a recent experiment [13], a different type of secondary electron emission detector was used to measure an antiproton beam emitted at much lower energies ($K = 10\text{--}120$ keV) from a radio frequency quadrupole decelerator. These measurements will be fully described in a separate publication.

Acknowledgements

I am indebted to the members of the ASACUSA and PS205 collaborations for their help and encouragement during this work. Techniques for manufacturing the patterned electrodes of the profile monitors were developed during the years

1994–1998 in collaboration with the Minotos Corporation of Tokyo, Japan. I would like to thank Y. Fujita, R. Hayano, H. Kumagai, and K. Mori for their help. This work was supported by two grants from Monbukagakusho of Japan: the Grant-in-Aid for Specially Promoted Research and for International Scientific Research, and the Grant-in-Aid for Creative Basic Research (10NP0101).

References

- [1] T. Yamazaki, N. Morita, R. Hayano, E. Widmann, J. Eades, Phys. Rep. 366 (2002) 183.
- [2] M. Hori, K. Yamashita, R.S. Hayano, T. Yamazaki, Nucl. Instr. and Meth. A 496 (2003) 102.
- [3] S. Baird, J. Bosser, M. Chanel, P. Lefèvre, R. Ley, D. Manglunki, S. Maury, D. Möhl, G. Tranquille, Hyperfine Interactions 76 (1993) 61.
- [4] M. Chanel, LEAR Performance, Proceedings of the LEAR Symposium, CERN, Geneva, 1998; M. Chanel, CERN/PS 99-040 (CA), CERN, Geneva, 1999.
- [5] T. Azuma, et al., Atomic spectroscopy and collisions using slow antiprotons, CERN/SPSC 97-19, CERN, Geneva, 1997.
- [6] M. Hori, Nucl. Phys. A 692 (2001) 119.
- [7] M. Hori, J. Eades, R.S. Hayano, T. Ishikawa, J. Sakaguchi, E. Widmann, H. Yamaguchi, H.A. Torii, B. Juhász, D. Horváth, T. Yamazaki, Phys. Rev. Lett. 87 (2001) 093401.

- [8] M. Hori, R.S. Hayano, E. Widmann, H.A. Torii, *Opt. Lett.* 28 (2003) 2479.
- [9] M. Hori, J. Eades, R.S. Hayano, T. Ishikawa, J. Sakaguchi, T. Tasaki, E. Widmann, H. Yamaguchi, H.A. Torii, B. Juhász, D. Horváth, T. Yamazaki, *Phys. Rev. Lett.* 89 (2002) 093401.
- [10] B. Juhász, J. Eades, R.S. Hayano, M. Hori, D. Horváth, T. Ishikawa, J. Sakaguchi, H.A. Torii, E. Widmann, H. Yamaguchi, T. Yamazaki, *Eur. Phys. J. D* 18 (2002) 261.
- [11] H. Yamaguchi, T. Ishikawa, J. Sakaguchi, E. Widmann, J. Eades, R.S. Hayano, M. Hori, H.A. Torii, B. Juhász, D. Horváth, T. Yamazaki, *Phys. Rev. A* 66 (2002) 022504.
- [12] E. Widmann, J. Eades, T. Ishikawa, J. Sakaguchi, T. Tasaki, H. Yamaguchi, R.S. Hayano, M. Hori, H.A. Torii, B. Juhász, D. Horváth, T. Yamazaki, *Phys. Rev. Lett.* 89 (2002) 243402.
- [13] M. Hori, J. Eades, R.S. Hayano, T. Ishikawa, W. Pirkel, E. Widmann, H. Yamaguchi, H.A. Torii, B. Juhász, D. Horváth, T. Yamazaki, *Phys. Rev. Lett.* 91 (2003) 123401.
- [14] S. Baird, et al., Design Study of the Antiproton Decelerator : AD, CERN/PS/96-43 (AR), CERN, Geneva, 1996.
- [15] T. Erikson, S. Maury, D. Möhl, *Nucl. Phys. A* 692 (2001) 187.
- [16] M. Mitani, private communication.
- [17] H. Stelzer, *Nucl. Instr. and Meth.* 133 (1976) 409.
- [18] U. Lynen, H. Stelzer, A. Gobbi, H. Saan, A. Olmi, *Nucl. Instr. and Meth.* 162 (1979) 657.
- [19] D. Swan, J. Yurkon, D.J. Morrissey, *Nucl. Instr. and Meth. A* 348 (1994) 314.
- [20] H. Kumagai, A. Ozawa, N. Fukuda, K. Sümmerer, I. Tanihata, *Nucl. Instr. and Meth. A* 470 (2001) 562.
- [21] H.W. Fulbright, *Nucl. Instr. and Meth.* 162 (1979) 21.
- [22] F. Sauli, Principles of Operation of Multiwire Proportional and Drift Chambers, CERN 77-09, CERN, Geneva, 1977.
- [23] V. Agoritsas, K. Kuroda, Monitoring beams of very low energy particles, Topical seminar on experimental apparatus for high energy particle physics and astrophysics, San Miniato, Tuscany, 1990;
- V. Agoritsas, K. Kuroda, CERN/PS/90-72 (PA), CERN, Geneva, 1990.
- [24] H. Saan, H. Damjantschitsch, D. Hebbard, J. Junge, D. Pelte, B. Povh, D. Schwalm, D.B. Tran Thoai, *Nucl. Instr. and Meth.* 124 (1975) 509.
- [25] Y. Sugaya, Y. Yamanoi, J. Chiba, Yu. Kiselev, M. Numajiri, H. Ochiishi, K.H. Tanaka, K. Yasuda, Y. Yoshimura, *Nucl. Instr. and Meth. A* 368 (1996) 635.
- [26] S. Palestini, et al., *Nucl. Instr. and Meth. A* 421 (1999) 75.
- [27] F. Sauli, *Nucl. Instr. and Meth. A* 386 (1997) 531.
- [28] B. Jean-Marie, V. Lepeltier, D. L'Hote, *Nucl. Instr. and Meth.* 159 (1979) 213.
- [29] T.Z. Kowalski, *Nucl. Instr. and Meth. A* 234 (1985) 521.
- [30] CERN PROGRAM LIBRARY CERNLIB version 96a, CERN, Geneva, 1996.
- [31] PHYSICS ANALYSIS WORKSTATION PAW version 2.08/14, CERN, Geneva, 1997.
- [32] J. Bosser, Measurements on the low-intensity beams of LEAR and the antiproton accumulator, Second European Workshop on Beam Diagnostics and Instrumentation for Particle Accelerators, Travemünde, 1995; J. Bosser, DESY M-9507, DESY, Hamburg, 1995; J. Bosser, CERN/PS/95-28 (BD), CERN, Geneva, 1995.
- [33] P. Lubiński, et al., *Phys. Rev. Lett.* 73 (1994) 3199.
- [34] M. Agnello, et al., *Phys. Rev. Lett.* 74 (1995) 371.
- [35] S.P. Møller, E. Uggerhøj, H. Bluhme, H. Knudsen, U. Mikkelsen, K. Paludan, E. Morenzoni, *Phys. Rev. A* 56 (1997) 2930.
- [36] J.F. Ziegler, The Stopping and Range of Ions in Matter, Pergamon Press, New York, 1985.
- [37] W.H. Barkas, W. Birnbaum, F.M. Smith, *Phys. Rev.* 101 (1956) 778.
- [38] D. Hasselkamp, H. Rothard, K.-O. Groeneveld, J. Kemmler, P. Varga, H. Winter, Particle Induced Electron Emission II, Springer, Heidelberg, 1992.
- [39] V. Chohan, M. Angoletta, M. Ludwig, O. Marquerssen, P. Odier, F. Pedersen, G. Tranquille, U. Raich, L. Soby, T. Spickermann, Beam measurement systems for the CERN Antiproton Decelerator (AD), Proceedings of the 2001 Particle Accelerator Conference, Chicago, 2001, IEEE Operations Center, Piscataway, 2001.